PERGAMON

International Journal of Heat and Mass Transfer 43 (2000) 179–189

International Journal of HEAT and MASS TRANSFER

www.elsevier.com/locate/ijhmt

Simultaneous heat and mass transfer during the ascension of superheated bubbles

F.B. Campos, P.L.C. Lage*

Programa de Engenharia Química, COPPE/UFRJ, CEP 21.945-970, C.P. 68502, Rio de Janeiro, Brazil

Received 21 April 1998; received in revised form 20 April 1999

Abstract

A model has been developed for the simultaneous heat and mass transfer during the ascension of superheated bubbles in a liquid column, allowing variable gas physical properties and bubble radius. A correction factor for isothermal gas hold-up correlations, based on bubble model results, has been derived in order to apply them to nonisothermal systems. Results for the bubble volume and the evaporated mass per bubble are used in the prediction of experimental data on gas hold-up and vaporization rate obtained in a direct contact evaporator with fairly good agreement. It has been shown that the constant property and constant bubble radius assumptions lead to overestimation of the vaporization rate and gas hold-up.

1. Introduction

Direct contact evaporation can be used for several applications [1], including solvent evaporation for solute extraction. The simplest direct contact evaporator is nothing more than a shallow bubble column operated nonisothermally through the injection of superheated gas. The heat and mass transfer processes occur simultaneously, heating and vaporizing the liquid phase. The vapor is generated at the interface, transferred to the interior of the ascending bubbles which ultimately leave the column, carrying the produced vapor. Thus, the solution for the heat and mass transfer problem in a superheated bubble is the basis for modeling direct contact evaporators [2].

The bubble residence time is usually divided into two stages: its formation at a submerged orifice and its ascension through the continuous liquid phase. Several models have been developed to estimate the frequency of formation and the bubble size at the end of the formation stage for conditions with no heat or mass transfer. Among those, the Davidson and Schüler models [3,4] and the Gaddis and Vogelpohl model [5] join simplicity and sufficient accuracy for usual applications. The bubble residence time during the ascension stage is determined from its ascension velocity and column height. The ascension velocity is usually calculated from the force balance on the ascending bubble, using a convenient correlation for the drag coefficient [6,7] and, when necessary, a correction factor for the population effect [8], or simply from an empirical correlation for the bubble swarm velocity [9], or even from the definitions of the gas hold-up and superficial velocity [10]. It should be noted that the population correction factor depends on the gas hold-up. The column height also depends on the gas hold-up, which can be estimated from correlations for isothermal operation of bubble columns [11,12].

Most of the models developed for the heat and mass transfer problem in superheated bubbles have neglected these processes during the formation stage of the

* Corresponding author. Tel.: +55-21-590-2241; fax: +55-21-290-6626.

E-mail address: paulo@peq.coppe.ufrj.br (P.L.C. Lage)

0017-9310/00/$ - see front matter
PII: S0017-9310(99)00143-X

Nomenclature

A	coefficient in rule for constant property evaluation
B	transfer number, $C_{p_{ref}}(T_R - T_0)/L_1$
c	dimensionless mixture heat capacity, $C_p/C_{p_{ref}}$
c_i	dimensionless mean specific heat of component i, $\overline{C^0_{p_i}}/C_{p_{ref}}$
C_p	specific heat at constant pressure
D	mass diffusivity
f	frequency of bubble formation
h	heat transfer coefficient
H	specific enthalpy
L	latent heat of vaporization
Le	Lewis number, α/D
m	evaporated mass per bubble
$\dot{m}$	bubble vaporization rate
M	mass flow rate
$\dot{M}$	evaporator vaporization rate
N_{Bi}	Biot number, hR_F/λ_{ref}
N	number of orifices
q	diffusive heat flux
Q	volumetric flow rate
r	radius coordinate
R	radius
t	time
T	temperature
T_R	reference temperature for θ definition ($T_R = T_L$ when $T_0 \neq T_L$)
U	bubble ascension velocity
v	radial velocity
V	volume
Y	mass fraction
z	axial coordinate
Z	bubble column height
W	radial diffusion velocity

Greek symbols

α	thermal diffusivity
β	dimensionless radius, $R(t)/R_F$
γ	dimensionless density, ρ/ρ_{ref}
Γ	dimensionless vaporization rate, $\dot{m}/4\pi R_F \rho_{ref} \alpha_{ref}$
ε	gas hold-up
η	dimensionless radial coordinate, $r/R(t)$
θ	dimensionless temperature, $(T - T_0)/(T_R - T_0)$
ϑ	dimensionless radial velocity, $R_F v/\alpha_{ref}$
κ	dimensionless thermal conductivity, λ/λ_{ref}
λ	thermal conductivity
ρ	density
τ	dimensionless time, $\alpha_{ref} t/R_F^2$
Ψ	dimensionless mass diffusivity, D/D_{ref}

Subscripts

exp	experimental
F	bubble formation
g	gas
hyp	hypothetical bubbling process
i	species i (1 for water and 2 for air)
L	liquid
orif	orifice
r	residence, at the end of bubble ascension
ref	reference state to evaluate physical properties for dimensionless variable definitions
S	surface
0	initial

Superscripts

$\underline{\ }$	mean property
0	pure component

bubble [13–15], even though there is experimental evidence that most of the bubble superheat is transferred during this stage [16]. In these models, the bubble is assumed to be instantaneously formed at the volume predicted by a bubble formation model without heat and mass transfer [3–5]. Some approximated analytical solutions have been developed for the simultaneous heat and mass transfer during the formation of superheated bubbles by simplifying the problem using a mean value for the bubble radius [17] or by, a priori, assuming that its transient behavior is known during the formation stage [18]. However, these models still use the approximation of constant physical properties for the gas phase which may lead to erroneous predictions for the final bubble radius and evaporated mass per bubble.

During the formation and ascension of a superheated bubble, the bubble mass increases due to the vaporization but the bubble density increases as the temperature drops to that of the liquid phase. The static pressure also decreases during the bubble ascension, but its effect on the gas density is much smaller than the temperature change for the usual column heights found in direct contact evaporators. Thus, the bubble radius would change during the formation and ascension stages, which can only be predicted by allowing

variable physical properties. The bubble radius changes also affect the gas hold-up, which is considerably overestimated by the isothermal correlations [14].

This work has developed a comprehensive model for the simultaneous heat and mass transfer during the ascension of superheated bubbles which allows variable properties for the gas phase and considers the interdiffusion term in the energy conservation equation. The bubble is assumed spherical and to be instantaneously formed at the final formation volume predicted by the Davidson and Schüler model [3]. During bubble formation, the heat and mass transfer is neglected in the present model. Since the time dependence of the bubbles radius is part of the solution, this is actually a free boundary problem. The main objectives are to evaluate the accuracy of the constant property and constant bubble radius assumptions and to use the model results to interpret available experimental data of direct contact evaporation. Thus, a simplified analysis is used to develop a correction factor for gas hold-up isothermal correlations which is able to explain the discrepancy between experimental gas hold-up values and their predictions through the isothermal correlations [14]. Moreover, the model predictions for the vaporized mass per bubble with and without the constant property assumption are used to obtain the values for the vaporization rate which are then compared to the experimental data.

2. Heat and mass transfer model

The complete description for the heat and mass transfer phenomena associated with the ascension of a superheated bubble should take into account the simultaneous solution of the continuity, momentum, energy and chemical species conservation equations. In order to simplify the problem, it is assumed that the internal pressure gradient is very small, so that the momentum conservation equation does not have to be solved. Since small column heights are usually employed in direct contact evaporators, this constant pressure assumption introduces only a few percent error in the model results.

The continuity, energy and species conservation equations for a multicomponent mixture, as shown in Ref. [19], can be simplified to Eqs. (1)–(3), shown below, by using the following hypotheses: the bubble is spherical, there is spherical symmetry with no circulation inside the bubble, the hydrostatic liquid column head is neglected in order to consider the pressure inside the bubble constant during the whole process, the gas phase is an ideal binary mixture of water vapor and air (or any other pseudo-component), there is liquid–vapor equilibrium at the bubble surface, there is no heat source, the viscous dissipation term is neglected and the gravity is the only existing field force.

$$\frac{\partial \rho}{\partial t} + \frac{1}{r^2}\frac{\partial}{\partial r}\left(r^2 \rho v\right) = 0 \tag{1}$$

$$\frac{\partial}{\partial t}(\rho Y_i) + \frac{1}{r^2}\frac{\partial}{\partial r}\left[r^2 \rho Y_i (v - W_i)\right] = 0 \tag{2}$$

$$\frac{\partial}{\partial t}(\rho H) + \frac{1}{r^2}\frac{\partial}{\partial r}\left(r^2 \rho v H\right) + \frac{1}{r^2}\frac{\partial}{\partial r}\left(r^2 q\right) = 0 \tag{3}$$

The diffusive fluxes, including the interdiffusion heat transport, are given by

$$q = -\lambda\frac{\partial T}{\partial r} + \sum_{i=1}^{2} \rho H_i^0 Y_i W_i, \quad W_i = -\frac{D_i}{Y_i}\frac{\partial Y_i}{\partial r} \tag{4}$$

The boundary conditions at the bubble surface for Eqs. (1)–(3) are given by the mass and energy surface balances, which can be derived from the conservation equations through a limit process [19] and are expressed as

$$-\frac{\dot{m}}{4\pi R^2} = \rho_S\left(v_S - \frac{\mathrm{d}R}{\mathrm{d}t}\right), \quad r = R(t) \tag{5}$$

$$\rho_S D_S \left.\frac{\partial Y_1}{\partial r}\right|_{r=R(t)} = \frac{\dot{m}}{4\pi R^2}\left(1 - Y_{1_S}\right), \quad r = R(t) \tag{6}$$

$$-\lambda \left.\frac{\partial Y_1}{\partial r}\right|_{r=R(t)} = \frac{\dot{m}}{4\pi R^2} L_1(T_S) + h(T_S - T_L), \quad r = R(t) \tag{7}$$

For the binary ideal-gas mixture, the specific enthalpy is given by

$$H(T) = \sum_{i=1}^{2} Y_i H_i^0(T) \tag{8}$$

Assuming constant mean specific heats for the gas-phase components over the whole domain of temperature, the energy conservation equation can be transformed to

$$\frac{\partial}{\partial t}\left(\rho C_p T\right) + \frac{1}{r^2}\frac{\partial}{\partial r}\left(r^2 \rho v C_p T\right) = \frac{1}{r^2}\frac{\partial}{\partial r}\left(r^2 \lambda \frac{\partial T}{\partial r}\right) + \left(\overline{C_{p_1}^0} - \overline{C_{p_2}^0}\right)\frac{1}{r^2}\frac{\partial}{\partial r}\left(r^2 T \rho D \frac{\partial Y_1}{\partial r}\right) \tag{9}$$

Since the specific heats of the gas phase components do not depend strongly on temperature, this hypothesis has very little effect on the model predictions.

Since there is no circulation inside the bubble, the radial velocity is caused by the bubble dilation. Thus,

it can be calculated from the integration of the continuity equation [20]:

$$v(r,t) = -\frac{1}{r^2\rho(r,t)}\int_0^r \frac{\partial \rho(\xi,t)}{\partial t}\xi^2\,\mathrm{d}\xi \tag{10}$$

The heat and mass transfer model is completed by predictions of the bubble formation diameter, bubble formation frequency, bubble ascension velocity, bubble–liquid heat transfer coefficient and interfacial equilibrium. For the bubble formation diameter and frequency estimates, the correlation of Davidson e Schüler [3] has been used, due to its simplicity and accuracy for low viscosity solutions. The bubble is assumed to be always at the terminal ascension velocity of an isolated bubble, which has been calculated through the Karamanev correlation [7], using the liquid properties evaluated at the bulk liquid temperature, except for the viscosity and the surface tension, which are calculated at the film temperature. Due to the small gas hold-up values experimentally observed in direct contact evaporators, no population correction factor is applied to the ascension velocity. The bubble–liquid heat transfer coefficient was estimated by the heat and mass transfer analogy and the Calderbank and Moo-Young correlation for mass transfer from small bubbles [21]. The interfacial equilibrium is determined from Raoult's law and from the Wagner's equation for the water vapor pressure [22].

Experimental data for the physical properties of the gas phase components (water and air) [23] were correlated by Lage and Rangel [24] as functions of temperature and pressure. These correlations for the specific heat, dynamic viscosity, thermal conductivity, water latent heat of vaporization and for the binary diffusion coefficient have been used in this work. The density of the gas mixture was given by the ideal gas law. The gas mixture specific heat was obtained from the ideal solution behavior and the mixture thermal conductivity was estimated by the Wassiljewa's [22]. The mean specific heat values for the mixture components, which have been used to simplify the energy conservation equation, were obtained from the mean specific heat definition, using the gas inlet temperature and the liquid temperature as the limits in the integration process:

$$\overline{C_{\mathrm{p}_i}}^{0} = \frac{1}{T_0 - T_\mathrm{L}}\int_{T_\mathrm{L}}^{T_0} C_{\mathrm{p}_i}^{0}\,\mathrm{d}T \tag{11}$$

3. Gas hold-up in nonisothermal systems

The usual correlations for gas hold-up estimation [11,12] do not give good predictions for nonisothermal bubble columns, as in the case of direct contact evaporators [14]. It is believed that the discrepancies between experimental results and predictions are mainly due to the nonisothermal behavior of the superheated bubble during its formation and ascension through the column. Although the previously described numerical model includes only the bubble ascension stage, the reasoning for a general correction procedure for gas hold-up estimation in nonisothermal systems is developed below. The basic idea is to incorporate a correction factor to well-known correlations for gas hold-up.

From the gas hold-up definition, it can be derived that

$$\frac{V_\mathrm{g}}{V_\mathrm{L}} = \frac{\varepsilon}{1-\varepsilon} \tag{12}$$

where the liquid phase volume can be considered invariant for a hypothetical bubbling process where there is no heat and mass transfer and for the actual nonisothermal process at the same liquid and gas temperatures. On the other hand, the gas phase volume is obtained from the mean bubble volume, the number of orifices in the gas distribution system, the mean frequency of bubble formation at these orifices, f_orif, and the mean bubble residence time, as shown below.

$$V_\mathrm{g} = \overline{V} f_\mathrm{orif} N t_\mathrm{r} = \overline{V} f t_\mathrm{r} \tag{13}$$

where f is the bubble formation frequency in the column.

Using Eqs. (12) and (13) for both the hypothetical and nonisothermal processes in a bubble column with the same liquid and gas phase temperatures and the same liquid volume, we can derive

$$\frac{\varepsilon}{1-\varepsilon} = \frac{\overline{V} f_\mathrm{orif}\ t_\mathrm{r}}{\left(\overline{V} f_\mathrm{orif} t_\mathrm{r}\right)_\mathrm{hyp}}\left(\frac{\varepsilon}{1-\varepsilon}\right)_\mathrm{hyp} \tag{14}$$

where 'hyp' indicates the hypothetical bubbling process with no heat or mass transfer.

The bubble volume, the frequency of bubble formation and the bubble residence time are different for the hypothetical and nonisothermal processes due to the heat and mass transfer during the superheated bubble formation and ascension. Using the model described in the last section, the effect of the heat and mass transfer can be evaluated only during the bubble ascension stage. Thus, no information of this effect on the frequency of bubble formation can be obtained. However, the bubble volume and residence time can be evaluated by the present model for the hypothetical and nonisothermal processes, giving rise to a correction factor in the form

$$\frac{\varepsilon}{1-\varepsilon} = \overline{\beta}^3 \frac{t_r}{t_{r_{hyp}}} \frac{\varepsilon_{hyp}}{1-\varepsilon_{hyp}} \tag{15}$$

where $\overline{\beta}$ is the mean dimensionless bubble radius during the ascension stage given by

$$\overline{\beta} = \frac{1}{Z}\int_0^Z \beta(z)\,dz \tag{16}$$

In the bubble residence time evaluation, a homogeneous bubbling regime is assumed. The residence time for the hypothetical case is simply given by $Z/U_{hyp} + t_F$, where U_{hyp} is the bubble ascension velocity relative to a fixed frame of reference and is calculated using the bubble formation radius, R_F, and t_F is the time for bubble formation ($t_F = 1/f_{orif}$). For the nonisothermal case, the model uses the bubble ascension velocity to determine the bubble instantaneous location during its ascension and, consequently, the bubble residence time. Thus, for a bubble column in a semi-batch operation, the residence time of the bubble is calculated by

$$z(t_r) = \int_{t_F}^{t_r} U\,dt = Z \tag{17}$$

where U is approximated by the terminal velocity of the bubble using its instantaneous conditions.

Since the column height, Z, depends on the gas hold-up, the correction factor for the gas hold-up correlation given by Eq. (15) has to be calculated by iteration when Z is not known. Moreover, the heat and mass transfer processes usually occur quite early in the bubble residence time, enabling the usage of the final value of β, β_r, in the place of $\overline{\beta}$ to obtain an approximated value for the correction factor. This substitution cannot be done for very shallow columns.

4. Numerical procedure

In order to simplify the numerical solution of the free boundary problem given by Eqs. (1), (2), (5)–(7) and (9), the physical domain was transformed to a computational fixed domain through the definition of a new radial coordinate, η, and a new dimensionless radius, β. Using several dimensionless variables which are defined in the Nomenclature, the dimensionless conservation equations and their boundary conditions can be written as:

$$\frac{\partial \gamma}{\partial \tau} - \frac{\eta}{\beta}\frac{d\beta}{d\tau}\frac{\partial \gamma}{\partial \eta} + \frac{1}{\eta^2\beta}\frac{\partial}{\partial \eta}\left(\eta^2 \gamma \vartheta\right) = 0 \tag{18}$$

$$\begin{aligned}&\frac{\partial}{\partial \tau}(\gamma Y_1) - \frac{\eta}{\beta}\frac{d\beta}{d\tau}\frac{\partial}{\partial \eta}(\gamma Y_1)\\ &+\frac{1}{\eta^2\beta}\frac{\partial}{\partial \eta}\left[\eta^2 \quad \gamma\left(Y_i\vartheta - \frac{\Psi}{\beta Le_{ref}}\frac{\partial Y_1}{\partial \eta}\right)\right] = 0\end{aligned} \tag{19}$$

$$\begin{aligned}&\frac{\partial}{\partial \tau}(\gamma c\theta) - \frac{\eta}{\beta}\frac{d\beta}{d\tau}\frac{\partial}{\partial \eta}(\gamma c\theta)\\ &+\frac{1}{\eta^2\beta}\frac{\partial}{\partial \eta}\left[\eta^2\left(\gamma c\theta\vartheta - \frac{\kappa}{\beta}\frac{\partial \theta}{\partial \eta}\right)\right] - (c_1 - c_2)\frac{1}{\eta^2\beta}\frac{\partial}{\partial \eta}\\ &\left(\eta^2 \frac{\gamma \Psi \theta}{Le_{ref}\beta}\frac{\partial Y_1}{\partial \eta}\right) = 0\end{aligned} \tag{20}$$

$$-\frac{\Gamma}{\beta^2} = \gamma_S\left(\vartheta_S - \frac{d\beta}{d\tau}\right), \quad \eta = 1 \tag{21}$$

$$\frac{\gamma_S \Psi_S \beta}{Le_{ref}}\frac{\partial Y_1}{\partial \eta}\bigg|_{\eta=1} = \Gamma\left(1 - Y_{1_S}\right), \quad \eta = 1 \tag{22}$$

$$-\frac{\kappa}{\beta}\frac{\partial \theta}{\partial \eta}\bigg|_{\eta=1} = \frac{\Gamma}{\beta^2 B} + N_{Bi}(\theta_S - \theta_L), \quad \eta = 1 \tag{23}$$

The numerical model given by Eqs. (18)–(23) has been solved by the method of lines using finite-volume spatial discretization. Eqs. (19) and (20) have been discretized in η coordinate using a staggered nonuniform grid, where the velocity grid points are placed at the volume interfaces. The power-law interpolation function given by Patankar [25] was used to evaluate the convective-diffusive terms. When it was necessary, this scheme was slightly modified to calculate the values of the dependent variables at the volumes interfaces. The terms where $d\beta/d\tau$ appears explicitly and the interdiffusion term in the energy equation have been incorporated in the source terms of the discretization scheme [25]. The boundary conditions given by Eqs. (22) and (23), and the symmetry conditions at the bubble center are directly incorporated in the discretized equations. The integration of Eq. (18) over the η coordinate allows the calculation of the dimensionless radial velocity profile inside the bubble as soon as the dimensionless temperature and concentration profiles are calculated during the simulation. The resulting system of nonlinear ordinary differential equations have been numerically integrated using the DASSL routine [26], with automatic error control. Typically, an absolute tolerance of 10^{-8} and a relative tolerance of 10^{-6} have been used in the mixed tolerance convergence criterion of DASSL. Eqs. (16) and (17) were integrated using the trapezoidal rule in order to determine β and t_r. The final value for the mass of vaporized water, m_r,

was also calculated through trapezoidal integration along the transient simulation of the bubble ascension. Enough time intervals were taken to obtain these values with an accuracy better than 1%.

5. Results and discussion

Table 1 shows the conditions used in the simulations whose results will be discussed below. In the simulation cases 1 to 5, the gas is ejected at the same mass flow rate through very small orifice diameters in order to generate bubbles that can be adequately approximated by spheres. Cases 6 and 7 are related to the experimental conditions utilized by Queiroz [14], whose data in Table 1, except R_F, are taken from the experiments. The corresponding equivalent bubble radius values, R_F, calculated by the Davidson e Schüler correlation [3], are also shown in Table 1. Preliminary evaluations of gas-phase physical properties at T_L and T_0 have shown large variations. Gas density changes are equal to 180% for case 2, 203% for case 6 and 115% for case 7. Thermal conductivities of water vapor and air vary about 70, 60 and 45% and mass diffusivities of these components change around 85, 90 and 75%, for cases 2, 6 and 7, respectively. On the other hand, specific heat changes with temperature are only about 10–15% and have been neglected in the model. Thus, a large variable property effect is to be expect for the cases shown in Table 1.

In the conditions of case 1, there is no mass or heat transfer and this case has been used to check the consistency of the developed numerical model, which behaved as physically expected, with no change of temperature, water concentration or bubble radius. The conditions of case 2 have been used to show the convergence characteristics of the numerical model, which are shown in Fig. 1 for the dimensionless radius and for the mass of vaporized water. It can be seen that convergence in the space discretization has been achieved by using 161 finite volumes in a nonuniform grid. This large number of finite volumes is necessary

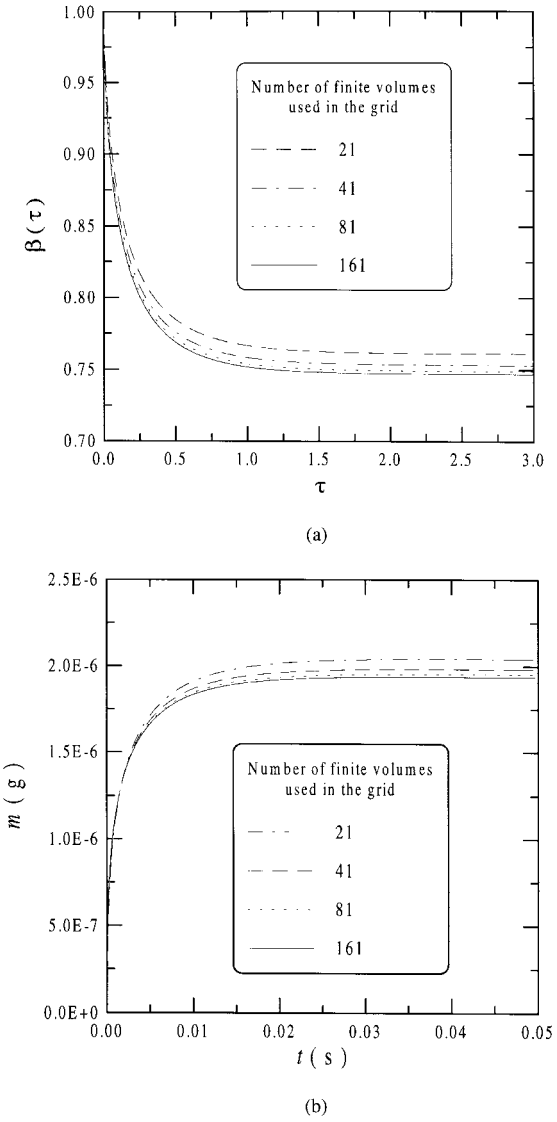

Fig. 1. Convergence analysis: (a) dimensionless radius and (b) mass of vaporized water.

Table 1
Conditions used in the simulations

Case	T_0 (K)	T_L (K)	Y_{1_0} (%)	Q_{orif} (cm^3/s)	M_{orif} (mg/s)	R_{orif} (mm)	R_F (mm)
1	323	323	7.97	1.000	1.038	0.1	1.76
2	900	323	1.96	2.689	1.038	0.1	1.76
3	900	353	1.96	2.689	1.038	0.1	1.76
4	600	323	1.96	1.793	1.038	0.1	1.76
5	600	353	1.96	1.793	1.038	0.1	1.76
6	1066	350	7.59	56.8	17.9	0.65	8.88
7	742	350	7.59	39.5	17.9	0.65	7.70

due to the extremely steep gradients that are developed near the bubble surface.

The effects of considering variable properties and the interdiffusion term in the energy equation were analyzed for the conditions of case 2 given in Table 1. Fig. 2 shows some results for the complete numerical model developed in this work (variable properties), for this model with the interdiffusion term eliminated from the energy equation by imposing the hypothesis of equal specific heats for the two components, water vapor and air, (constant C_p) and for the same model with all the physical properties considered constant (constant properties). For the constant C_p case, the mixture specific heat was evaluated at conditions given by the mean arithmetic temperature and water vapor concentration between the gas inlet and the gas–liquid equilibrium conditions. For the constant property simulations, all properties but the gas density have been evaluated at convenient mean conditions given by $\overline{T} = T_0 - A(T_0 - T_L)$ and $\overline{Y}_1 = Y_{1_0} - A(Y_{1_0} - Y_1^*)$, where Y_1^* is the water vapor equilibrium concentration at T_L. The one-third rule ($A = 1/3$) has shown to be better than the arithmetic mean ($A = 1/2$), as will be seen in the following. The gas density is evaluated at T_0 and Y_{1_0} in order to keep consistency with the bubble formation model that uses this gas density value.

Fig. 2 shows the transient behaviors of the dimensionless bubble radius and the mass of vaporized water and the radial profiles of the dimensionless temperature, the water vapor mass fraction and the dimensionless radial velocity. From these results, it can be seen that the effect of the interdiffusion term is small for the conditions analyzed. Simulations for other initial conditions have also shown the same behavior leading to the conclusion that this term can be neglected in the energy equation. On the other hand, the consideration of constant properties seriously overestimates the bubble radius and the mass of vaporized water.

Fig. 3 shows the effect of the continuous and dispersed phase temperatures on the transient behavior of the mass of vaporized water in the conditions of cases 2–5 of Table 1. While a 300 K increase in the initial gas temperature leads to an enhance of 9% in the mass of vaporized water, a 30 K raise in the liquid temperature is responsible for a 730% increase in the mass of vaporized water. This kind of behavior is typical for gas–liquid systems where the interfacial equilibrium is a nonlinear function of temperature.

Due to the lack of other experimental data on direct contact evaporation in the reviewed literature, the analysis of the gas hold-up and vaporization rate in nonisothermal systems is restricted to Queiroz [14] experimental data. Moreover, Queiroz [14] presented data only for a narrow range of operational conditions of the direct contact evaporator, which can be characterized by cases 6 and 7 of Table 1.

Actually, cases 6 and 7 refer to one set of experimental conditions used by Queiroz [14], where the liquid column height was 55.8 cm. The initial temperature of 1066 K (case 6) represents the gas temperature measured by a thermocouple located approximately at 150 cm after the gas burner and about 80 cm ahead of the gas distribution system. In case 7, the gas initial temperature of 742 K is a corrected temperature, obtained from an energy balance considering thermal losses through the gas admission tube and using a radiation correction for the thermocouple reading. It is worth to say that, in obtaining the value for the corrected temperature, the thermocouple radiant properties were estimated. Since the value of the correction factor is quite dependent on the thermocouple emissivity, large errors may exist in the correct temperature. Thus, both the actual temperature reading and the corrected temperature are used in the following analysis. The evaporator used by Queiroz [14] has 57 cm in diameter with a gas distribution system composed by 288 orifices, each one with 0.65 mm in diameter.

Although Queiroz [14] has fed the evaporator with combustion gas, the calculations shown in the following analysis have been carried out using the physical properties of a water vapor–air mixture. This implies in considering that the residual oxygen and the produced carbon dioxide have properties similar to those of nitrogen. A comparison of specific heats at constant pressure and thermal conductivities allows the estimation of the error involved in this approximation to be around 3–4%.

The developed model does not allow the prediction of the volume with which the bubble begins its ascension. Since the gas distribution system of the direct contact evaporator was built with special care to allow that the bubble formation occurs in the constant flow rate regime [14], the Davidson and Schüler model [3] was used to determine the bubble formation volume from the volumetric flow rate of the injected gas accounting for the residual gas volume at the orifice.

Table 2 shows some results obtained by the numerical model for the superheated bubble ascension, using variable properties or constant properties with different rules to evaluate $\overline{T}$ and $\overline{Y}_1$, that enables the calculation of the correction factor for isothermal gas hold-up correlations as given by Eq. (14). From Table 2, it can be seen that the values of the dimensionless bubble mean radius, $\overline{\beta}$, and those for the dimensionless bubble radius at the end of the process, β_r, are practically equal. As commented above, this occurs because the largest rates of heat and mass transfer take place in the beginning of the process, enabling the use of the β_r value to calculate the gas hold-up correction factor. However, in this case the column height is known ex-

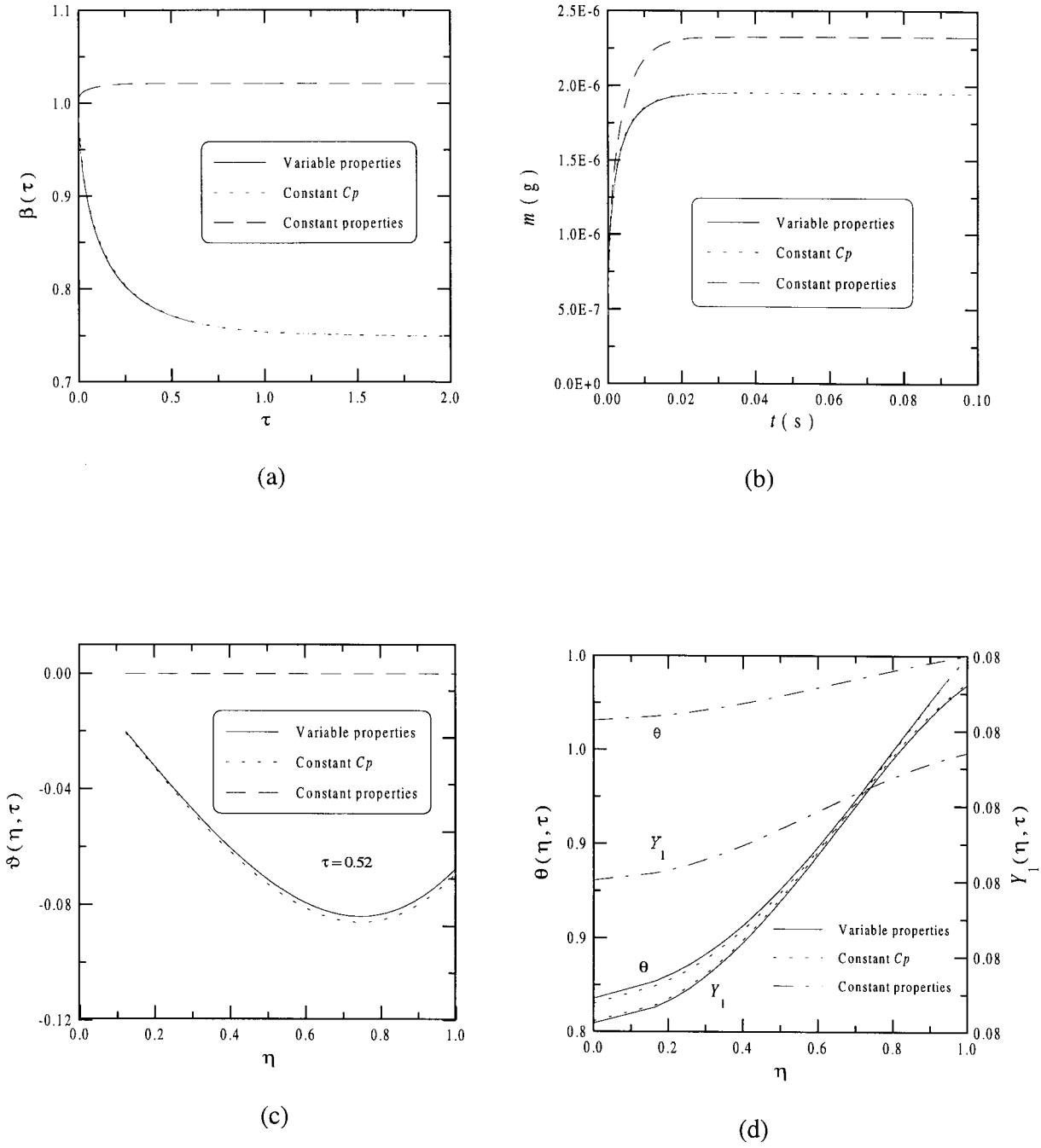

Fig. 2. Effects of considering variable properties and the interdiffusion term in the energy equation: (a) transient behavior of the dimensionless radius, (b) transient behavior of the mass of vaporized water, (c) dimensionless radial velocity profiles and (d) dimensionless temperature and concentration profiles.

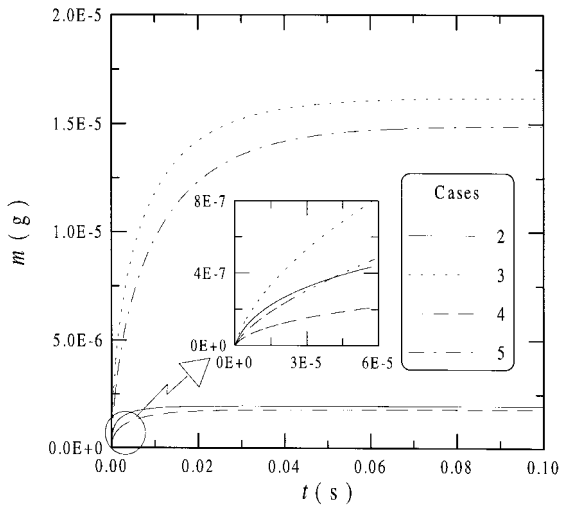

Fig. 3. Effect of injected gas temperature and liquid phase temperature in the mass of vaporized water per bubble.

perimentally and $\overline{\beta}$ can be determined by the numerical model without iteration.

Comparing the dimensionless radii at the end of the process for cases 6 and 7 obtained with the variable property assumption, given in Table 2, it can be seen that the largest bubble contraction, observed by the smallest value for β_r, occurs for the largest initial temperature and it is due to the accentuated increase of the gas density caused by bubble temperature reduction.

In Table 2, ε_{exp} is the experimental value of the gas hold-up and ε_{hyp} represents the value obtained from two gas hold-up correlations using the gas initial conditions (Akita and Yoshida [11] and Hikita et al. [12]) that assume no heat and mass transfer. The corrected gas hold-up calculated by Eq. (14), is given by ε for each one of these correlations. It should be noted that the ε_{hyp} value is the gas hold-up estimate for superheated bubble models that do not allow bubble radius changes caused by the heat and mass transfer process.

Table 2
Correction factor analysis for gas hold-up correlations[a]

Case	$\overline{\beta}$	β_r	t_r (s)	Akita and Yoshida ε_{hyp}	Akita and Yoshida ε	Hikita et al. ε_{hyp}	Hikita et al. ε
Variable properties							
6	0.820	0.809	2.064	0.141	0.091	0.132	0.085
7	0.919	0.912	2.121	0.112	0.094	0.107	0.089
Constant properties at $\overline{T}$ and $\overline{Y}_1$ with $A = 1/2$, except ρ (at T_0 and Y_{1_0})							
6	1.096	1.099	1.793	0.141	0.172	0.132	0.162
7	1.095	1.099	1.918	0.112	0.138	0.107	0.131
Constant properties at $\overline{T}$ and $\overline{Y}_1$ with $A = 1/3$, except ρ (at T_0 and Y_{1_0})							
6	1.097	1.099	1.794	0.141	0.172	0.132	0.162
7	1.096	1.099	1.918	0.112	0.138	0.107	0.131
$\varepsilon_{exp} = 0.05 \pm 0.03$							

[a] $t_{r_{hyp}}$ (case 6) = 1.872 s and $t_{r_{hyp}}$ (case 7) = 2.004 s.

For the Akita and Yoshida [11] and Hikita et al. [12] correlations are the most commonly used for gas hold-up estimation in bubble columns. Originally developed for isothermal conditions, they fail to predict the value of the gas hold-up in nonisothermal bubble columns as can be seen in Table 2, where the predicted gas hold-up value closest to the experimental value, which is between 2 and 8%, is the 10.7% value obtained by the Hikita et al. correlation [12] in the conditions of case 7.

From Fig. 2a, when the gas phase properties are considered constant, the bubble radius suffers a small increase due to the water vapor formation. This effect is also seen in Table 2 for the constant property cases, where $\overline{\beta} > 1$. For each case, although the residence time decreases ($t_r < t_{r_{hyp}}$) due to the larger bubble size, the resulting correction factor implies an increase in the gas hold-up values in relation to those predicted by the correlations. Thus, comparing the ε_{hyp} and ε values to the ε_{exp} value, the constant property and constant bubble radius assumptions lead to a severe overestimation of the gas hold-up. For the gas hold up evaluation, the rule used to evaluate $\overline{T}$ and $\overline{Y}_1$ is immaterial.

For the variable property simulations, the correction factor based on the change of bubble residence time and on the bubble volume reduction, both due to the heat and mass transfer process, leads to smaller values for the gas hold-up. Using this correction factor, the maximum predicted value for ε is 9.4%, and the minimum one is 8.5%. These values are not yet within the experimental error range obtained by Queiroz [14]. However, the correction factor reduces the value predicted for the gas hold-up towards the low values experimentally observed. The error in the gas hold-up predictions drops from 114–180% to 70–88% with the usage of the correction factor. This indicates that the effect of heat and mass transfer on the bubble residence time and on the bubble volume are partially responsible for these low experimental gas hold-up values in nonisothermal bubble columns. It is believed that a change in the bubble frequency caused by the heat and mass transfer process during the bubble formation stage, which has been neglected in this work, should be responsible for a further decrease in the predicted gas hold-up values.

Table 3 shows the final values for the mass of vaporized water per bubble, m_r, for the experimental conditions of cases 6 and 7, obtained by the numerical

model with and without the constant property assumption using two rules for $\overline{T}$ and $\overline{Y}_1$. The frequency of bubble formation at all orifices of the gas distribution system, f, is the total volumetric flow rate divided by the bubble formation volume. The theoretical global mass vaporization rate in the direct contact evaporator, $\dot{M}$, is the product of the evaporator bubble frequency by the mass of vaporized water per bubble. In Table 3, the experimental quasi-steady value for the global mass vaporization rate, $\dot{M}_{exp}$, is presented with its experimental error which is basically due to the imprecision in the measurement of the water level changes in the evaporator. Comparing the results obtained through the simulations of cases 6 and 7 with variable properties to the experimental value, it can be noted that the model is predicting a vaporization rate 16% larger than the experimental value. However, if the 10% experimental error associated with the inlet gas flow rate measurement is taken into account, the results agree with the experimental data. This can be seen by reducing the inlet gas flow rate in 10%, which results in $\dot{M}$ predictions of 5.85 kg/h for case 6 and 5.83 kg/h for case 7. On the other hand, the $\dot{M}$ predictions obtained using the constant property assumption using the rule with $A = 1/2$ are too high, being 54 and 38% larger than the experimental value for cases 6 and 7, respectively. This difference is too large to be explained by the gas flow rate experimental error. Using $A = 1/3$, the errors drop to 29 and 21% for cases 6 and 7, respectively, which shows why this rule for the mean property evaluation has been used before and considered better than the arithmetic mean. However, the constant property assumption is still worse than the variable property results.

Table 3
Evaporator mass vaporization rate prediction by the superheated bubble model

Case	6	7
V_F (cm^3)	2.94	1.91
Q_{orif} (cm^3/s)	56.8	39.5
f (10^6 bubbles/h)	20.1	21.4
Variable properties		
m_r (10^{-7} kg)	3.24	3.03
$\dot{M}$ (kg/h)	6.50	6.48
Constant properties at $\overline{T}$ and $\overline{Y}_1$ with $A = 1/2$, except ρ (at T_0 and Y_{1_0})		
m_r (10^{-7} kg)	4.28	3.62
$\dot{M}$ (kg/h)	8.61	7.74
Constant properties at $\overline{T}$ and $\overline{Y}_1$ with $A = 1/3$, except ρ (at T_0 and Y_{1_0})		
m_r (10^{-7} kg)	3.59	3.17
$\dot{M}$ (kg/h)	7.22	6.77
$\dot{M}_{exp}$ (kg/h) = 5.6 ± 0.5		

Comparing the predicted values for $\dot{M}$ using variable properties, it is clear that there is no difference in considering the actual temperature reading or the corrected temperature. While the higher temperature of the inlet gas leads to a larger mass of vaporized water per bubble, the smaller temperature originates smaller bubbles at the orifices, due to the volumetric flow correction, which results in a larger number of bubbles. These opposite effects tend to cancel each other in the $\dot{M}$ calculation. However, which temperature is chosen for the model simulation is important in the gas hold-up prediction, as can be seen in Table 2, where a 4–10% difference exists between the gas hold-up values calculated for cases 6 and 7. For the constant property simulations, the gas temperature change does lead to a 10% difference in the $\dot{M}$ values. This difference is due to the lack of bubble contraction in this case, which is larger when the inlet gas temperature is higher.

The usage of $\overline{T}$ and $\overline{Y}_1$ instead of T_0 and Y_{1_0} to evaluate ρ for the constant property simulations has shown to lead to almost the same results for $\dot{M}$ and ε. The rule given by $A = 2/3$ has also been tested but it has led to poorer results.

6. Conclusions

This work has developed a comprehensive model for the simultaneous heat and mass transfer during the ascension of superheated bubbles which allows variable properties for the gas phase. The model has been used to interpret gas hold-up and vaporization rate data for a direct contact evaporator. For the available experimental data, it has been shown that the gas hold-up and the quasi-steady mass vaporization rate can be fairly well predicted using the results simulated by the numerical model. The gas hold-up prediction is based on well-known correlations for isothermal bubble columns and on a correction factor developed in this work, which can be partially calculated from the present developed model. A superheated bubble model including the bubble formation stage is necessary to completely evaluate this correction factor, which can explain the discrepancy that still exists between simulated and experimental results.

Then, it was concluded that the discrepancies between experimental gas hold-up values in non-isothermal bubble columns and their predictions through isothermal correlations are due to the heat and mass transfer phenomena occurring in the superheated bubble. It has also been shown that the assumptions of constant gas phase properties and constant bubble radius in the superheated bubble model lead to erroneous gas hold-up predictions and to an overestimation of the mass vaporization rate.

Acknowledgements

The kind assistance of Prof. Queiroz in obtained the raw experimental data is gratefully acknowledge. The authors also acknowledge the financial support obtained from CNPq, grant number 520660/98-6.

References

[1] D. Bharatahn, Direct contact evaporation, in: F. Kreith, F. Boehm (Eds.), Direct Contact Heat Transfer, Hemisphere, New York, 1988, pp. 203–222.
[2] P.L.C. Lage, C.M. Hackenberg, Simulation and design of direct contact evaporators, in: Multiphase Transport and Particulate Phenomena, vol. 2, Hemisphere, New York, 1990, pp. 577–592.
[3] J.F. Davidson, B.O.G. Schüler, Bubbles formation at an orifice in an inviscid liquid, Trans. Instn. Chem. Engrs 38 (1960) 335–342.
[4] J.F. Davidson, B.O.G. Schüler, Bubbles formation at an orifice in a viscous liquid, Trans. Instn. Chem. Engrs 38 (1960) 144–154.
[5] E.S. Gaddis, A. Vogelpohl, Bubbles formation in quiescent liquids under constant flow conditions, Chem. Engng. Sci 41 (1986) 97–105.
[6] R. Clift, J.R. Grace, M.E. Weber. Bubbles Drops and Particles, Academic Press, New York, 1978, pp. 111–116, 204–207.
[7] D.G. Karamanev, Rise of gas bubbles in quiescent liquids, AIChE J 40 (1994) 1418–1421.
[8] E. Ruckenstein, On mass transfer in the continuous phase from spherical bubbles or drops, Chem. Eng. Sci 19 (1964) 131–146.
[9] J.F. Davidson, D. Harrison, in: Fluidized Particles, Cambridge University Press, Cambridge, 1963, p. 53.
[10] Y.T. Shah, B.G. Kelkar, S.P. Godbole, W.D. Deckwer, Design parameters estimations for bubble column reactors, AIChE J 28 (1982) 353–379.
[11] K. Akita, F. Yoshida, Bubble interfacial area and liquid phase mass transfer coefficient in bubble columns, Ind. Eng. Chem. Proc. Des. Dev 13 (1974) 84–91.
[12] H. Hikita, S. Asai, K. Tanigawa, K. Segawa, M. Kitao, Gas hold-up in bubbles columns, Chem. Eng. Journal 20 (1980) 59–67.
[13] C.M. Hackenberg, A.L. Andrade, Transient surface temperature of superheated bubbles, in: T.N. Veriroglu (Ed.), Particulate Phenomena and Multiphase Transport, vol. 1, Hemisphere, Washington, 1988, pp. 377–382.
[14] E.M. Queiroz, Transferência Simultânea de Calor e Massa em Processos de Borbulhamento, D.Sc. thesis, COPPE/UFRJ, Rio de Janeiro, Brazil, 1990.
[15] E.M. Queiroz, C.M. Hackenberg, On the transient heat and mass transfer modelling of direct contact evaporators, in: J. Padet, F. Arinç (Eds.), Transient Convective Heat Transfer—ICHMT, vol. 1, Begellhouse, New York, 1996, pp. 179–189.
[16] H. Schmidt, Bubble formation and heat transfer during dispersion of superheated steam in saturated water—part II: from superheated steam bubbles to saturated water during bubble formation, Int. J. Heat Mass Transfer 20 (1977) 647–854.
[17] A.D. Pinto, C.M. Hackenberg, Evaporação Interfacial Durante a Formação de Bolhas Superaquecidas em Orifícios, in: Proceedings of the 5th Brazilian Thermal Sciences Meeting (ENCIT), vol. 1, ABCM, São Paulo, Brazil, 1994, pp. 36–44.
[18] A.C. Mezavilla, C.M. Hackenberg, Transient heat and mass transfer during the formation of superheated spherical bubbles, in: J. Padet, F. Arinç (Eds.), Transient Convective Heat Transfer—ICHMT, vol. 1, Begellhouse, New York, 1996, pp. 409–420.
[19] K.K. Kuo, Principles of Combustion, Wiley, New York, 1986 (Chapter 3).
[20] P.L.C. Lage, R.H. Rangel, C.M. Hackenberg, Nonideal vaporization of a dilating binary droplet with variable properties, International Journal of Heat and Mass Transfer 36 (1993) 3731–3741.
[21] P.H. Calderbank, M.B. Moo-Young, The continuous phase heat and mass transfer properties of dispersions, Chem. Eng. Sci 16 (1961) 39–54.
[22] R.C. Reid, J.M. Praunitz, B.E. Poling, The Properties of Gases and Liquids, 4th ed, McGraw-Hill, New York, 1987 (Chapters 7 and 8).
[23] N.B. Vargaftik, Tables on the Thermophysical Properties of Liquids and Gases in Normal and Dissociated States, Wiley, New York, 1975.
[24] P.L.C. Lage, R.H. Rangel, On the role of internal radiation absorption in single droplet vaporization, Paper number AIAA-92-0106, AIAA, 1992.
[25] S.V. Patankar, Numerical Heat Transfer and Fluid Flow, McGraw-Hill, New York, 1980.
[26] L.R. Petzold, DASSL code, version 1989, L316, Computing and Mathematics Research Division, Lawrence Livermore National Laboratory, Livermore, 1989.